Supporting Information

Acetylene/Ethylene Separation and Solid-State Structural Transformation *via* [2+2] Cycloaddition Reactions in 3D Microporous Zn^{II} Metal–Organic Frameworks

Arpan Hazra, Aashima Jain, M. S. Deenadayalan, Stephen Adie Adalikwu and Tapas Kumar Maji*

Molecular Materials Laboratory, Chemistry and Physics of Materials Unit, School of Advanced Materials (SAMat), Jawaharlal Nehru Centre for Advanced Scientific Research, Jakkur, Bangalore, 560 064, India.

*To whom correspondence should be addressed. T. K. Maji: E-mail: tmaji@jncasr.ac.in; Tel: (+91)-80-2208-2826; Fax: (+91)-80-2208-2766.

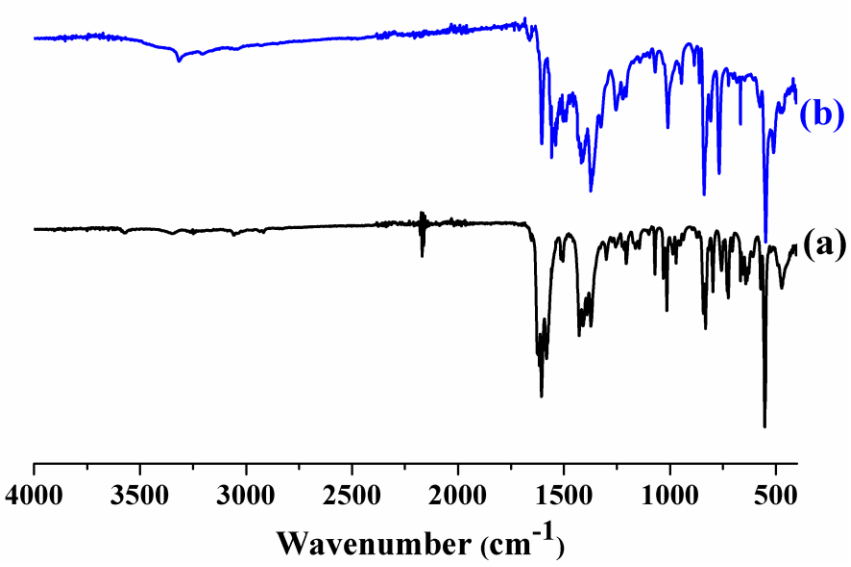

Figure S1: IR spectra of compounds **1** (a) and **1IR** (b).

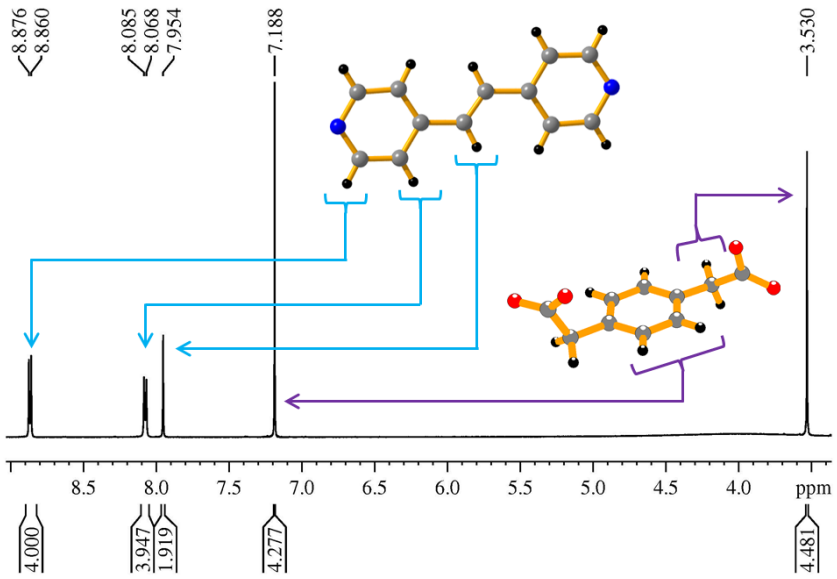

Figure S2: ^{1}H NMR spectra of **1** digested in DMSO-*d*6/DCl at 293 K. Two doublet signals at δ = (8.876, 8.860) and (8.085, 8.068) ppm are due to the hydrogen atoms of pyridine ring and a singlet at δ = 7.954 is due to the hydrogen atoms of ethylinic hydrogen atoms.. The presence of *pda* molecules is reflected from the signals at δ = 7.188 and 3.530.

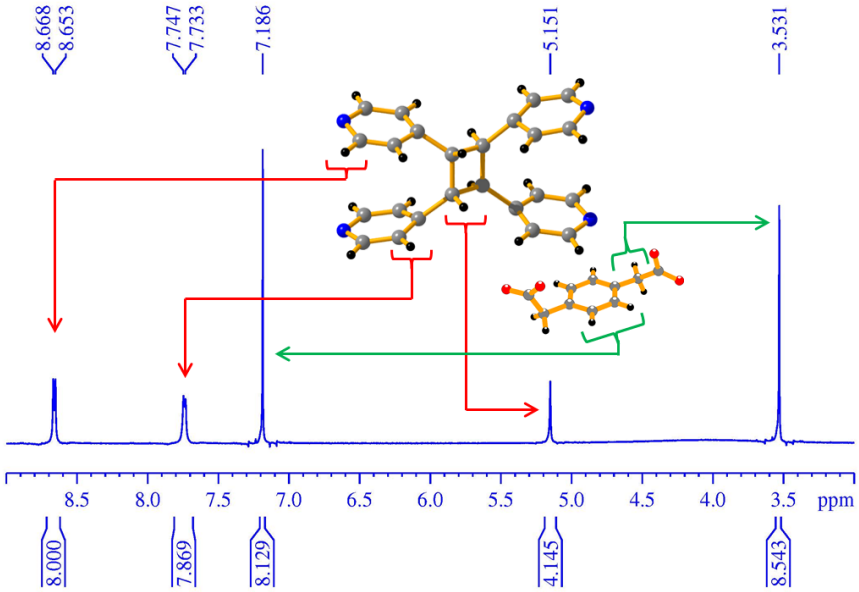

Figure S3: ^{1}H NMR spectra of **1IR** digested in DMSO-*d*6/DCl at 293 K. Two doublet signals at δ = (8.668, 8.653) and (7.747, 7.733) ppm are due to the hydrogen atoms of pyridine ring and a singlet at δ = 5.151 is due to the hydrogen atoms of cyclobutane ring. The presence of *pda* molecules is reflected from the signals at δ = 7.186 and 3.531.

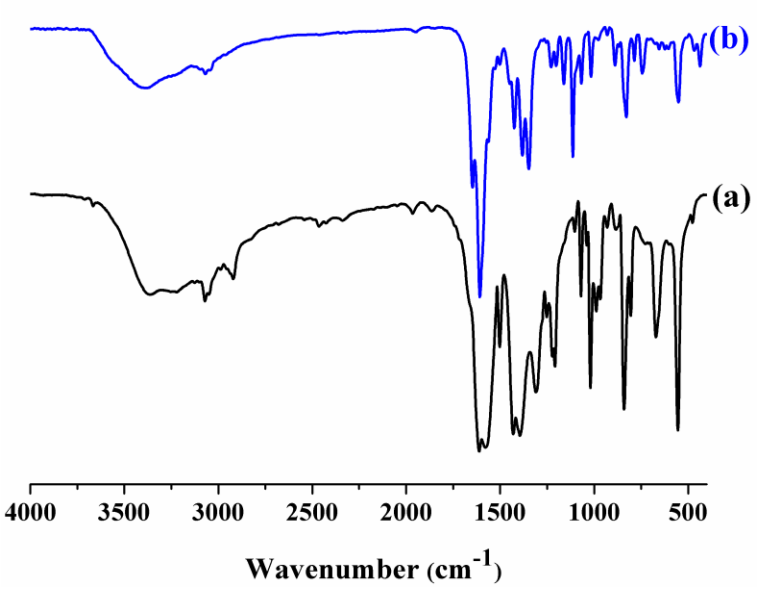

Figure S4: IR spectra of compounds **2** (a) and **2IR** (b).

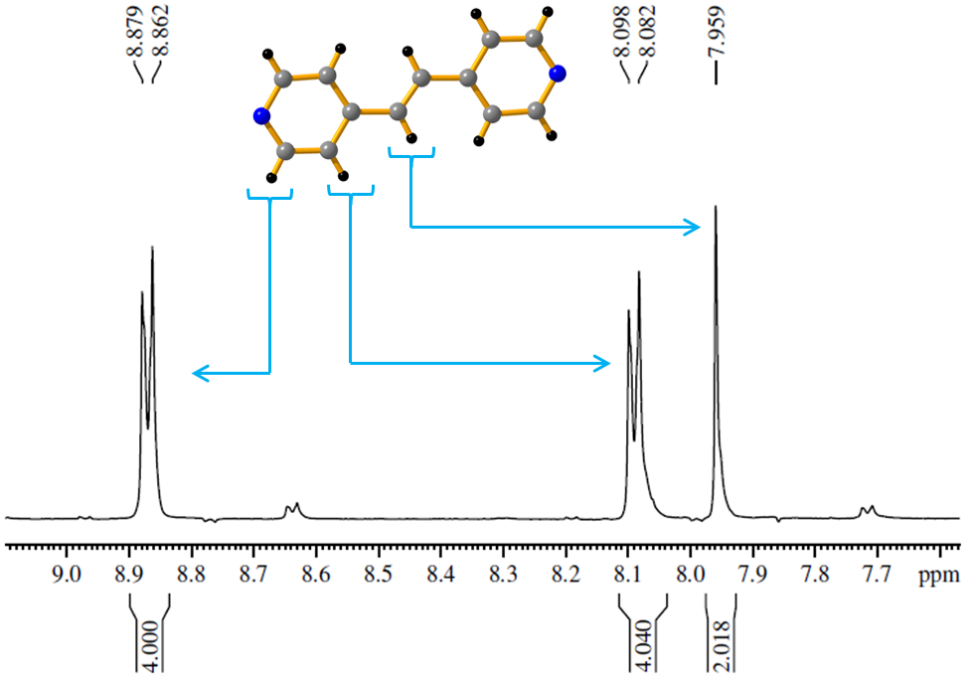

Figure S5: ^{1}H NMR spectra of **2** digested in DMSO-*d*6/DCl at 293 K. Two doublet signals at δ = (8.879, 8.862) and (8.098, 8.082) ppm are due to the hydrogen atoms of pyridine ring and a singlet at δ = 7.959 is due to the hydrogen atoms of ethylenic hydrogen atoms.

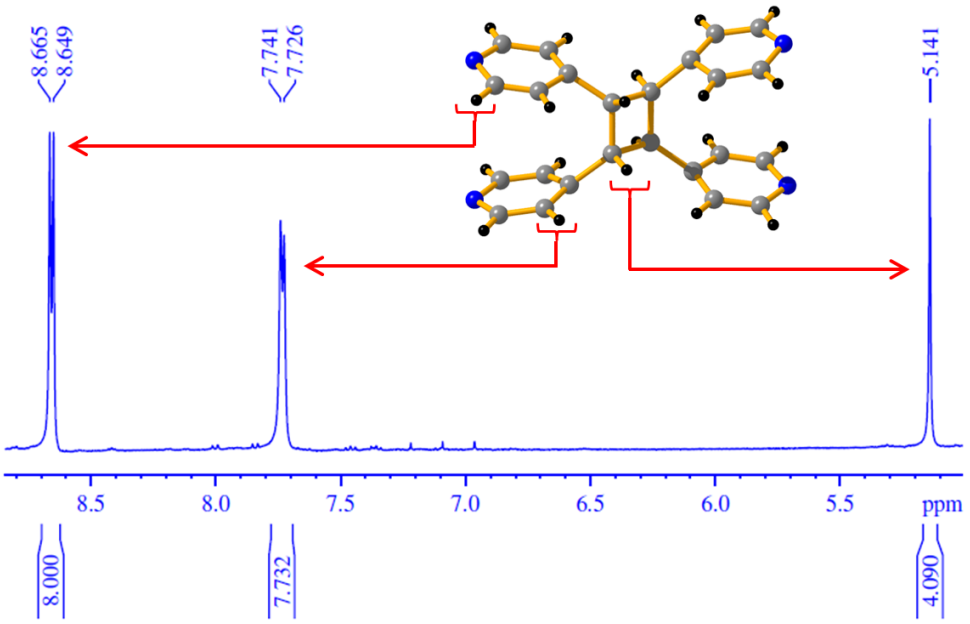

Figure S6: ^{1}H NMR spectra of **2IR** digested in DMSO-*d*6/DCl at 293 K. Two doublet signals at δ = (8.665, 8.649) and (7.741, 7.726) ppm are due to the hydrogen atoms of pyridine ring and a singlet at δ = 5.141 is due to the hydrogen atoms of cyclobutane ring.

Table S1. Crystal data and structure refinement for the compounds.

Identification code	**1**	**1IR**	**2**	**2IR**	**2_{LT}**	**$2IR_{LT}$**
Empirical formula	$C_{22}H_{18}N_2O_4Zn$	$C_{22}H_{18}N_2O_4Zn$	$C_{19}H_{25}N_2O_{10}Zn_2$	$C_{19}H_{25}N_2O_{10}Zn_2$	$C_{37}H_{38}N_4O_{21}Zn_4$	$C_{37}H_{38}N_4O_{21}Zn_4$
Formula weight	439.75	439.75	572.15	572.15	1136.15	1136.19
Temperature (K)	200(2)	150(2)	294(2)	293(2)	140(2)	140(2)
Wavelength (Å)	0.71073	0.71073	0.71073	0.71073	0.71073	0.71073
Crystal system	monoclinic	monoclinic	triclinic	triclinic	triclinic	triclinic
Space group	$P2_1/n$	$P2_1/n$	$P\bar{1}$	$P\bar{1}$	$P\bar{1}$	$P\bar{1}$
Unit cell dimensions (Å, °)	a = 10.4566(2) b = 13.3085(2) c = 13.7189(2) α = 90 β = 101.4910(10) γ = 90	a = 10.714(7) b = 13.167(4) c = 13.481(5) α = 90 β = 98.130(5) γ = 90	a = 8.5951(3) b = 9.9256(5) c = 14.2522(6) α = 104.312(2) β = 100.541(2) γ = 91.195(2)	a = 8.3953(5) b = 9.7690(7) c = 14.2096(11) α = 102.584(4) β = 101.421(4) γ = 92.328(4)	a = 9.9307(9) b = 14.3259(12) c = 16.9889(13) α = 100.845(3) β = 90.144(3) γ = 104.556(3)	a = 9.9197(5) b = 14.4346(7) c = 16.7116(8) α = 102.412(2) β = 91.240(2) γ = 103.880(2)
Volume (Å^3)	1870.88(5)	1882.7(15)	1155.47(9)	1110.58(14)	2294.4(3)	2261.94(19)
Z	4	4	2	2	2	2
Calculated density (g cm^{-3})	1.561	1.551	1.644	1.711	1.645	1.668
Absorption coefficient (mm^{-1})	1.346	1.337	2.132	2.218	2.149	2.180
F_{000}	904	904	586	586	1152	1152
Crystal size (mm^3)	0.140 × 0.100 × 0.080	0.140 × 0.100 × 0.080	0.130 × 0.100 × 0.080	0.150 × 0.100 × 0.080	0.140 × 0.100 × 0.080	0.140 × 0.100 × 0.080
θ range for data collection (°)	3.061 to 26.328	3.423 to 24.997	2.416 to 27.154	2.617 to 25.016	2.393 to 26.436	2.378 to 26.450
Miller index ranges	$-12 \le h \le 13$, $-16 \le k \le 16$, $-17 \le l \le 16$	$-12 \le h \le 12$, $-15 \le k \le 15$, $-16 \le l \le 16$	$-11 \le h \le 11$, $-12 \le k \le 12$, $-18 \le l \le 18$	$-9 \le h \le 9$, $-11 \le k \le 11$, $-16 \le l \le 16$	$-12 \le h \le 12$, $-17 \le k \le 17$, $-21 \le l \le 21$	$-12 \le h \le 12$, $-18 \le k \le 18$, $-20 \le l \le 20$
Reflections	27238	28597	22972	14149	53943	54400

collected						
Independent reflections	3784 [R_{int} = 0.0599]	3299 [R_{int} = 0.0709]	5099 [R_{int} = 0.0512]	3860 [R_{int} = 0.0644]	9363 [R_{int} = 0.0480]	9300 [R_{int} = 0.0555]
Completeness to θ_{max} (%)	0.994	0.995	0.997	0.988	0.993	0.997
Max. and min. transmission and Refinement method	Full-matrix least-squares on F^2	Full-matrix least-squares on F^2	Full-matrix least-squares on F^2	Full-matrix least-squares on F^2	Full-matrix least-squares on F^2	Full-matrix least-squares on F^2
Data / restraints / parameters	3784 / 12 / 281	3299 / 0 / 262	5099 / 36 / 318	3860 / 15 / 299	9368 / 152 / 678	9300 / 150 / 708
Goodness-of-fit on F^2	1.055	1.041	1.035	1.035	1.025	1.035
Final R indices [$I > 2\sigma(I)$]	$R1$ = 0.0363, $wR2$ = 0.0807	$R1$ = 0.0323, $wR2$ = 0.0785	$R1$ = 0.0405, $wR2$ = 0.0856	$R1$ = 0.0535, $wR2$ = 0.1187	$R1$ = 0.0341, $wR2$ = 0.0718	$R1$ = 0.0386, $wR2$ = 0.0877
R indices (all data)	$R1$ = 0.0492, $wR2$ = 0.0862	$R1$ = 0.0457, $wR2$ = 0.0871	$R1$ = 0.0606, $wR2$ = 0.0927	$R1$ = 0.0770, $wR2$ = 0.1290	$R1$ = 0.0470, $wR2$ = 0.0812	$R1$ = 0.0576, $wR2$ = 0.0958
Largest diff. peak and hole (e Å^{-3})	0.642 and -0.286	0.493 and -0.438	0.730 and -0.636	1.784 and -1.067	0.959 and -0.890	1.056 and -0.826

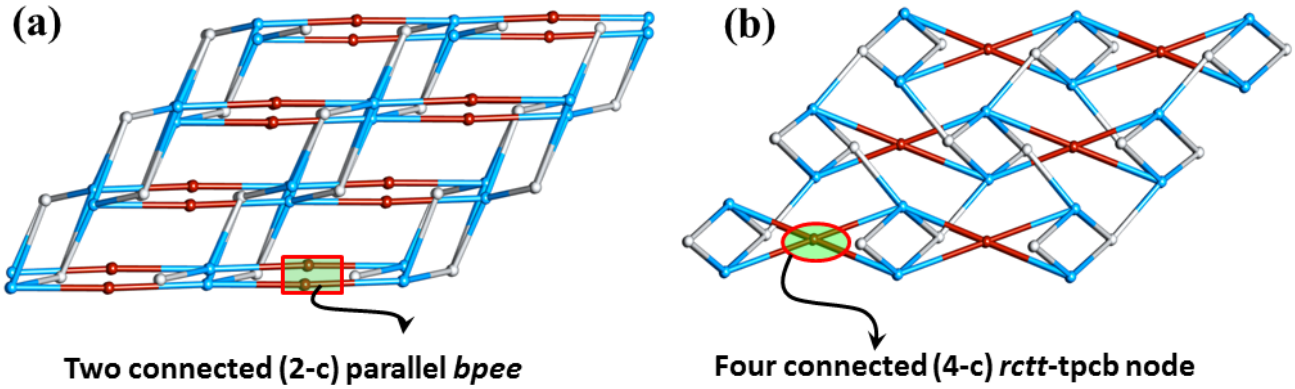

Figure S7: Network topology of **1** (a) and **1IR** (b) analyzed with TOPOS.[1]

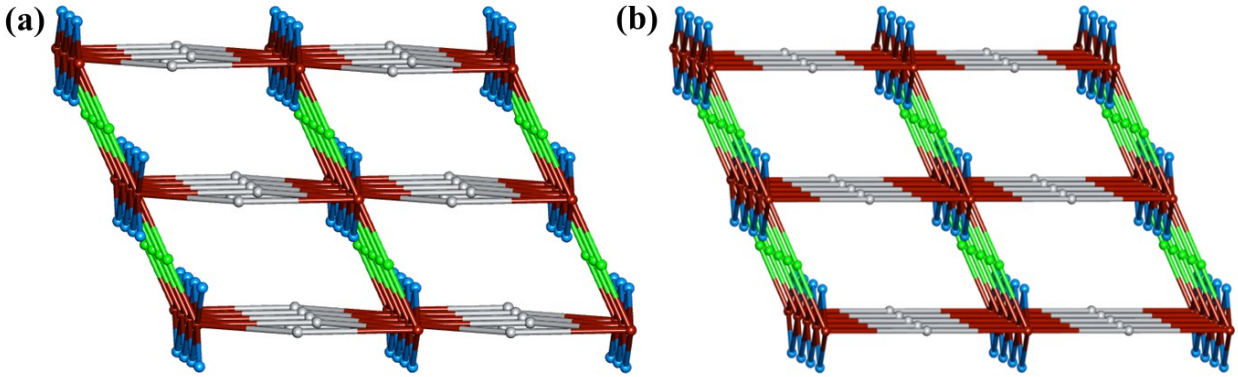

Figure S8: Network topology of **2** (a) and **2IR** (b) analyzed with TOPOS.[1]

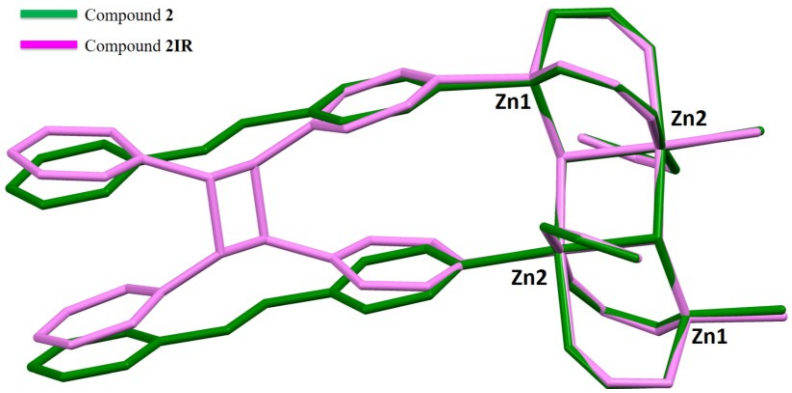

Figure S9: Structural overlay between compound **2** and **2IR** along the tetraneuclear SBU to show the movement of ethylinic carbon atoms and pyridine rings after photo-reaction.

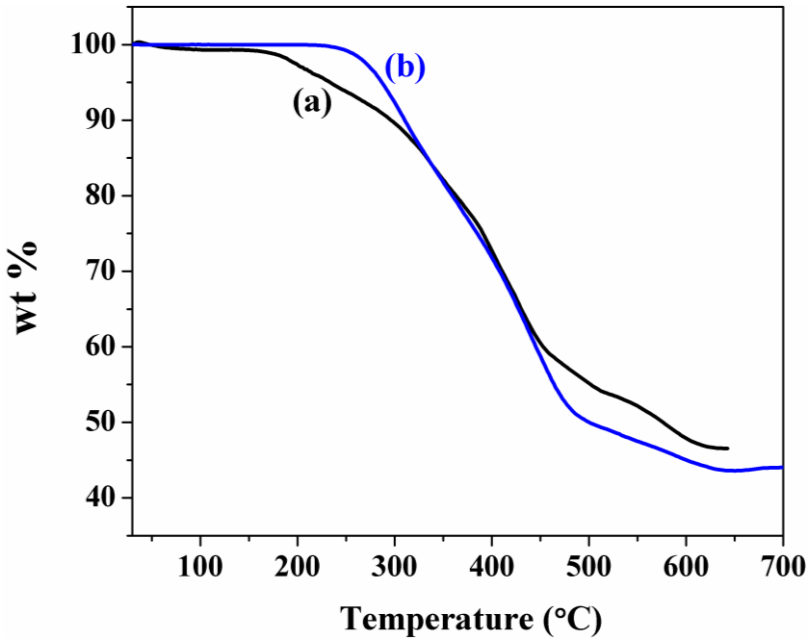

Figure S10: Thermogravimetric Analysis (TGA) of compound **1** (a) and **1IR** (b) in the temperature range of 25 to 700 °C (heating rate = 2°C min^{-1}) under N_2 atmosphere.

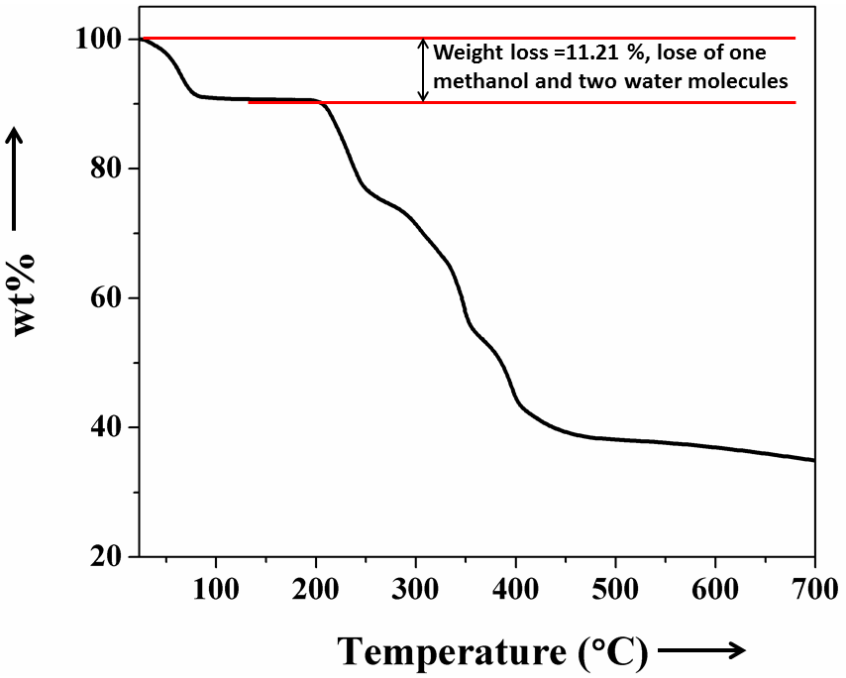

Figure S11: Thermogravimetric Analysis (TGA) of compound **2** in the temperature range of 25 to 700 °C (heating rate = 2°C min^{-1}) under N_2 atmosphere.

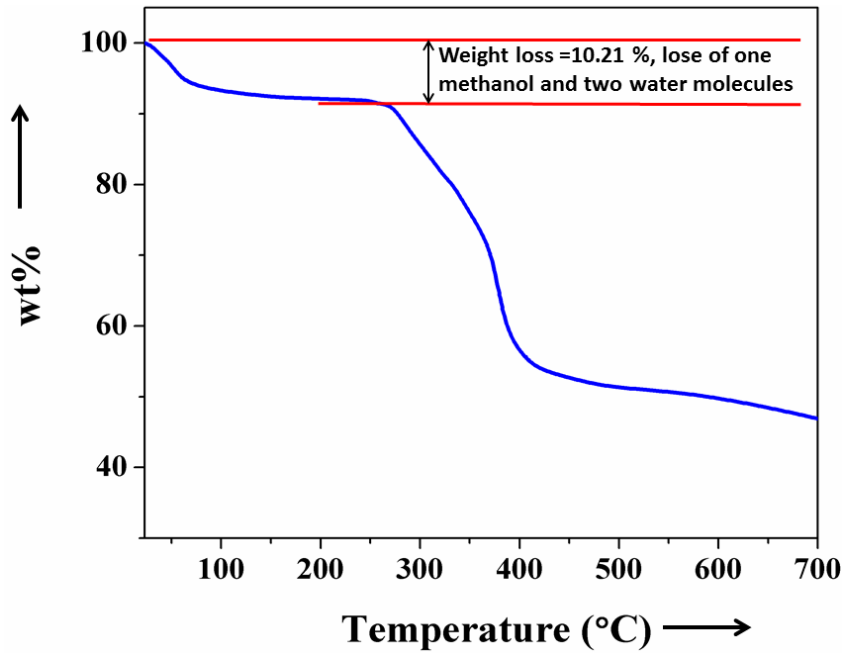

Figure S12: Thermogravimetric Analysis (TGA) of compound **2IR** in the temperature range of 25 to 700 °C (heating rate = 2°C min^{-1}) under N_2 atmosphere.

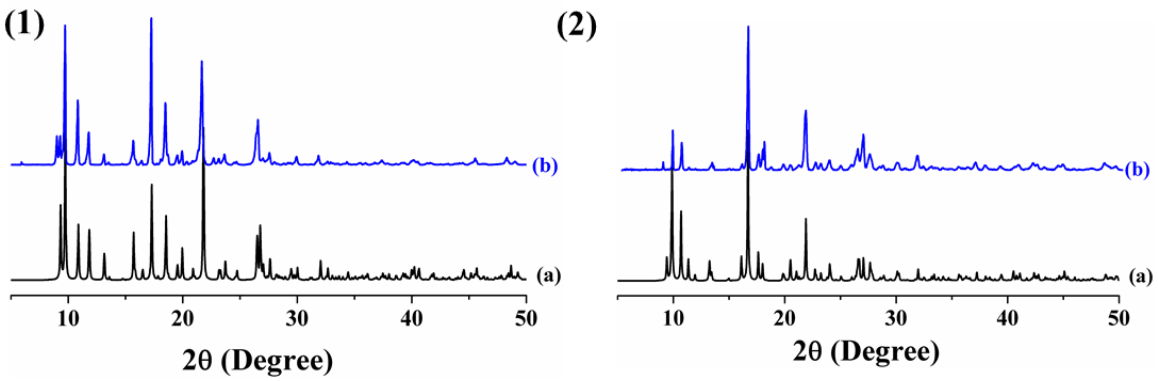

Figure S13. PXRD patterns of compounds **1** (1) and **1IR** (2) at different states; (a) Simulated (b) As-synthesized.

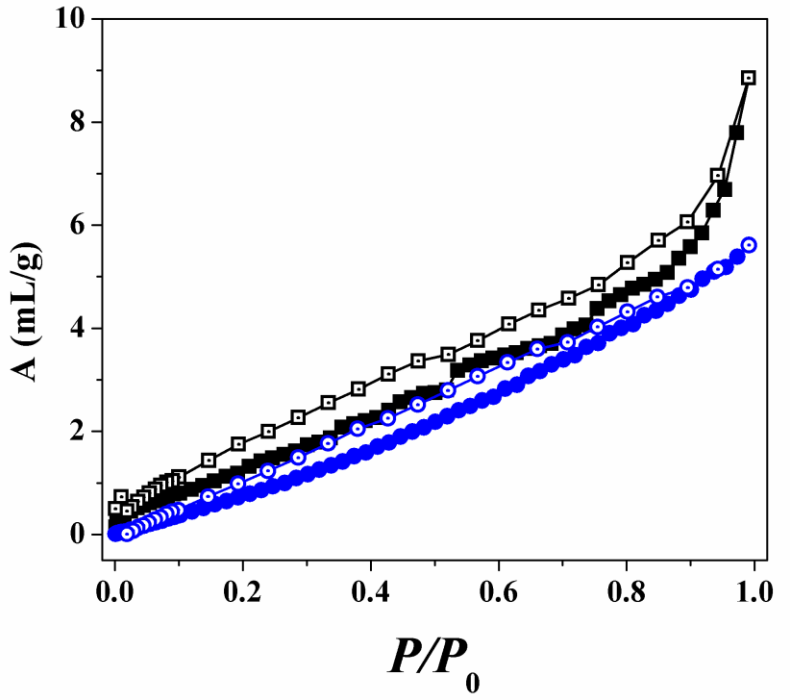

Figure S14: N_2 adsorption isotherms of compounds **2a** (black curve) and **2IRa** (blue curve) measured at 77 K. Open and closed symbols are representing adsorption and desorption respectively. P_0 = 680 torr.

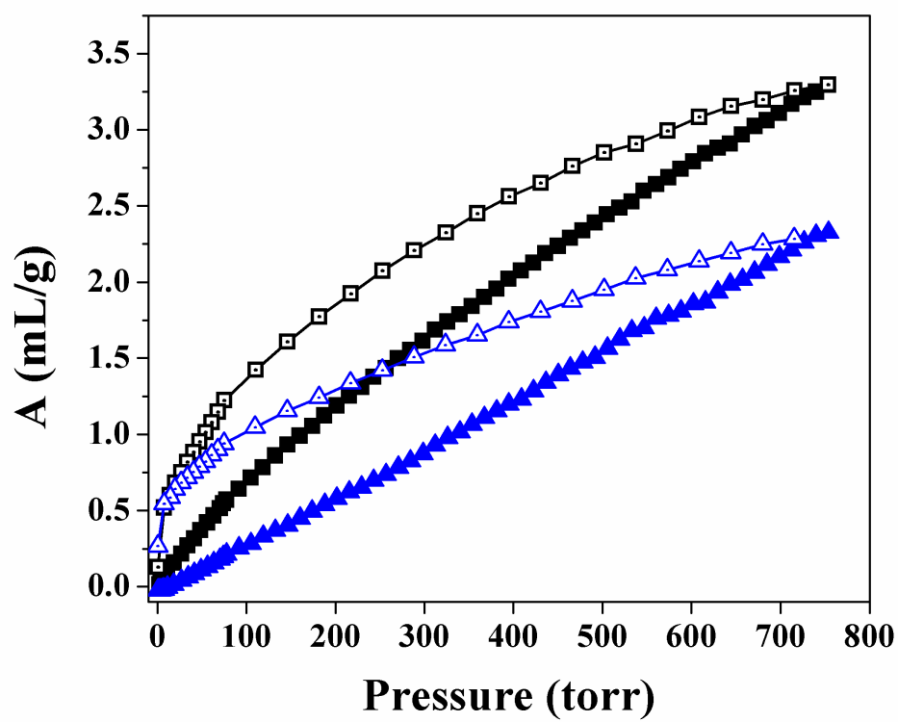

Figure S15: CO_2 adsorption isotherms of compounds **2a** (black curve) and **2IRa** (blue curve) measured at 273 K. Open and closed symbols are representing adsorption and desorption respectively. P_0 = 760 torr

S3.3.1. Analysis of Gas Adsorption Isotherms:

Heat of Adsorption (kJ mol^{-1}): We have used a virial type expression[2] of the following type to fit the combined isotherm data collected 283 and 293 K for C_2H_2.

$$\ln(P) = \ln(A) + \frac{1}{T}\sum_{i=0}^{m} a_i A^i + \sum_{i=0}^{n} b_i A^i \text{.....(2)}$$

Here, P is the pressure expressed in torr, A is the amount adsorbed in mmol/g, T is the temperature in K, a_i and b_i are virial coefficients, and m, n represent the number of coefficients required to adequately describe the isotherms. The values of m and n were gradually increased until the contribution of a and b coefficients added further were negligible towards the overall final fit. The values of the virial coefficient a_i were taken to calculate the isosteric heat of adsorption using the following expression.

$$Q_{st} = -R\sum_{i=0}^{m} a_i A^i \text{.....(3)}$$

Q_{st} is the coverage dependent isoteric heat of adsorption and R is the universal gas constant.

IAST Selectivity: The ideal adsorbed solution theory (IAST)[3-5] was used to predict the selectivity of C_2H_2 over CH_4, C_2H_4 and C_2H_6 gases. We employed the experimental pure-gas isotherms to calculate the selectivity. Previous reports have depicted that this method can predict the adsorption selectivity for mixture of isotherms in nanoporous materials, including metal-organic frameworks.[6-7] The single-component isotherms were fit to a single-site Langmuir-Freundlich equation.[4] The IAST assumes that the adsorbed phase is a two-dimensional solution in equilibrium with the bulk phase.[4] For binary adsorption of A and B, the IAST requires these two equations to be followed:

$$yP_t = xP_a \text{.....(4)}$$
$$(1-y)P_t = (1-x)P_b \text{.....(5)}$$

Where x and y denote the molar fraction of A in the adsorbed phase and the molar fraction of A in the bulk phase, respectively. P_t is the total gas pressure; P_a and P_b are the pressure of component A and B at the same spreading pressure as that of the mixture, respectively. The equation used for the fitting the single component gas mixture is as follows.

$$Y = Y_0\left(ln\frac{BP^n}{(1+BP^n)}\right) \text{.....(6)}$$

Furthermore, the molar fraction of A in the adsorbed phase can be obtained from the following equation:

$$Y_{0,a}\ln\left(1+\frac{B_aP_t^{n1}y}{x}\right) - Y_{0,b}\ln\left(1+\frac{B_bP_t^{n2}(1-y)}{(1-x)}\right) = 0 \text{.....(7)}$$

where $Y_{0,a}$, B_a and $n1$ are the Langmuir-Freundlich fitting parameters of adsorption equilibrium of pure A, $Y_{0,b}$, B_b and $n2$ are Langmuir-Freundlich parameters of adsorption equilibrium of pure B. The unknown x in Eq. (7) has been solved by Matlab (Version 7.8 (R2009a), The MathWorks, Inc.) for fixed P_t and y values.

Then calculated the predicted adsorption selectivity, which is defined as

$$S = \left(\frac{\frac{x_1}{y_1}}{\frac{x_2}{y_2}}\right) \text{.....(8)}$$

where x_i and y_i are the mole fractions of component i (i = 1, 2; A, B) in the adsorbed and bulk phases, respectively. The IAST calculations were carried out for a binary mixture containing 50-50 mixture of gases.

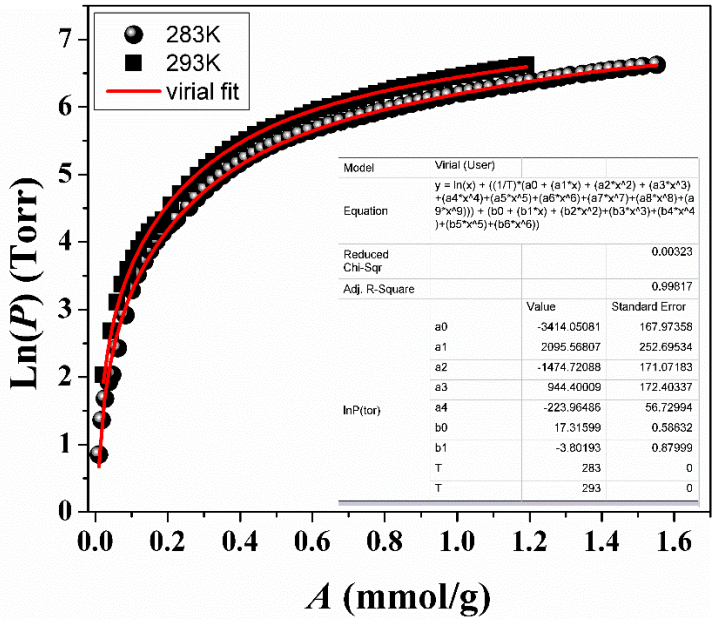

Figure S16: C_2H_2 isotherms for activated **2** (**2a**) measured at 283 K (black circle) and 293 K (black square). Fitted curves (red solid lines), obtained from the virial-type expansion, were used for the Q_{st} estimation.

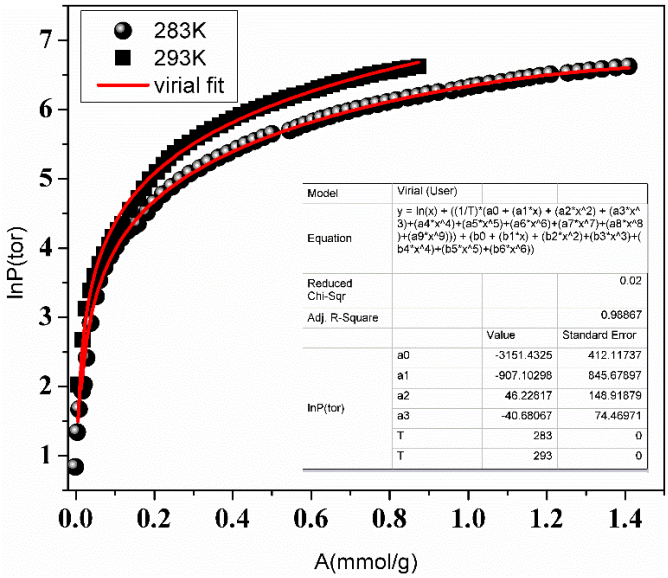

Figure S17: C_2H_2 isotherms for activated **2IR** (**2IRa**) measured at 283 K (black circle) and 293 K (black square). Fitted curves (red solid lines), obtained from the virial-type expansion, were used for the Q_{st} estimation.

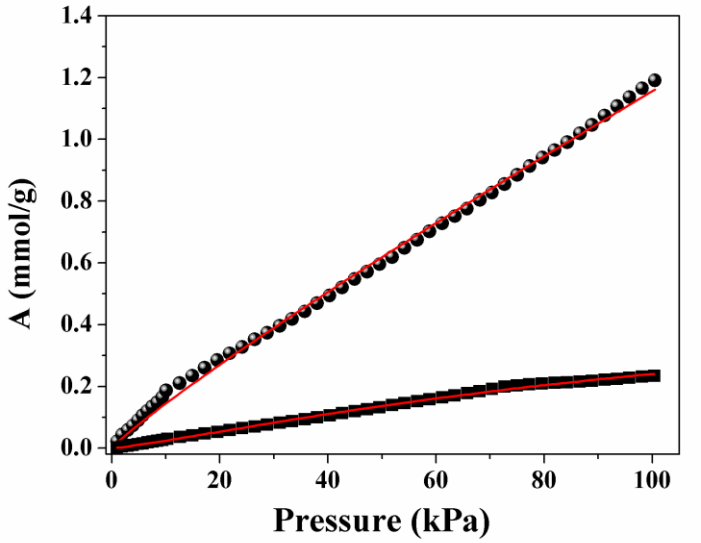

Figure S18: Langmuir-Freundlich fittings (red lines) for (a) C_2H_2 (black circle) and (b) C_2H_4 (black Square) isotherms measured at 293 K for **2a**.

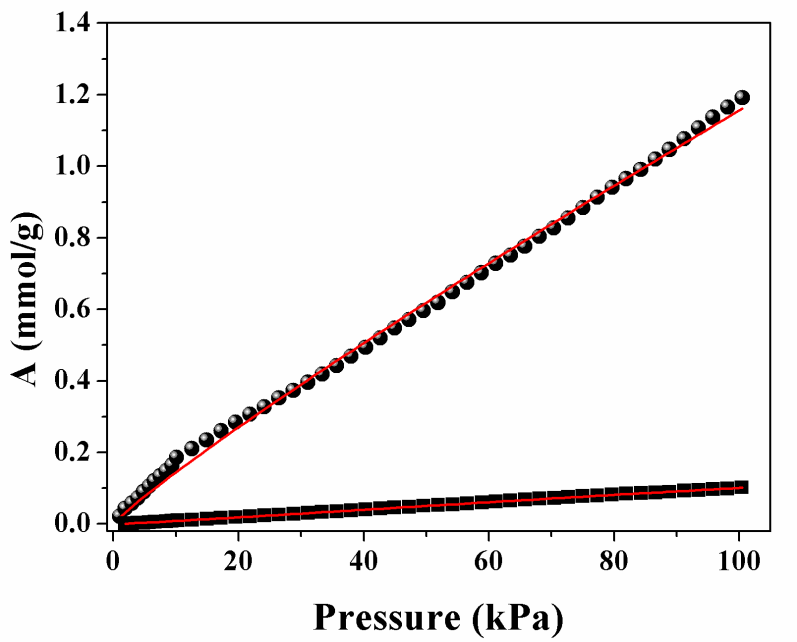

Figure S19: Langmuir-Freundlich fittings (red lines) for (a) C_2H_2 (black circle) and (b) C_2H_6 (black Square) isotherms measured at 293 K for **2a**.

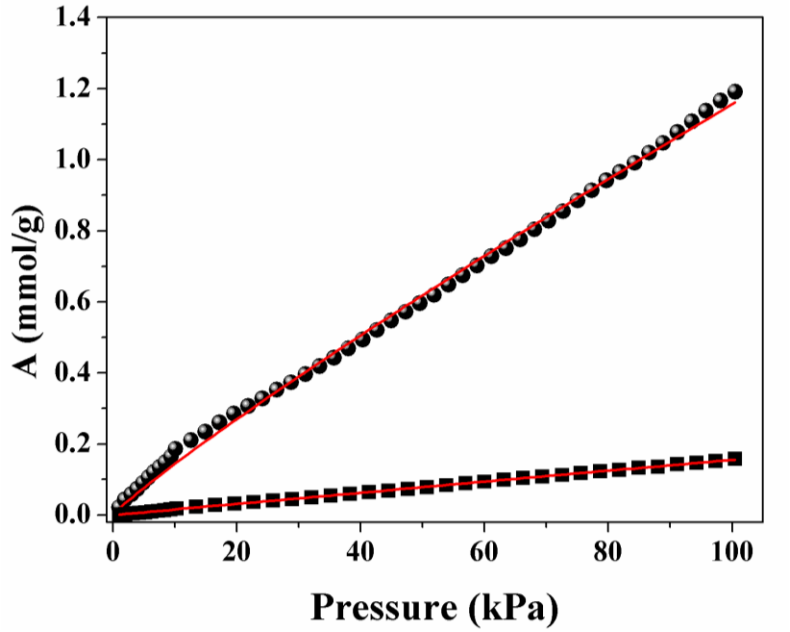

Figure S20: Langmuir-Freundlich fittings (red lines) for (a) C_2H_2 (black circle) and (b) CH_4 (black Square) isotherms measured at 293 K for **2a**.

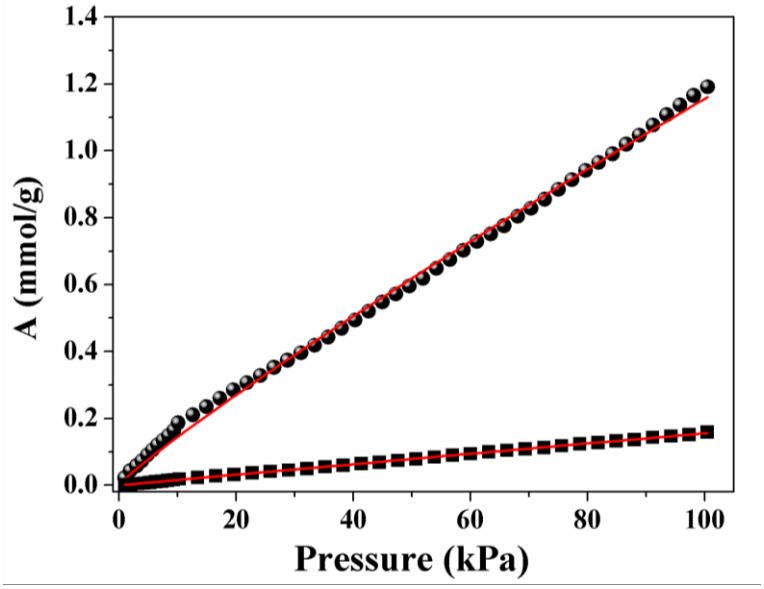

Figure S21: Langmuir-Freundlich fittings (red lines) for (a) C_2H_2 (black circle) and (b) C_2H_4 (black Square) isotherms measured at 293 K for **2IRa**.

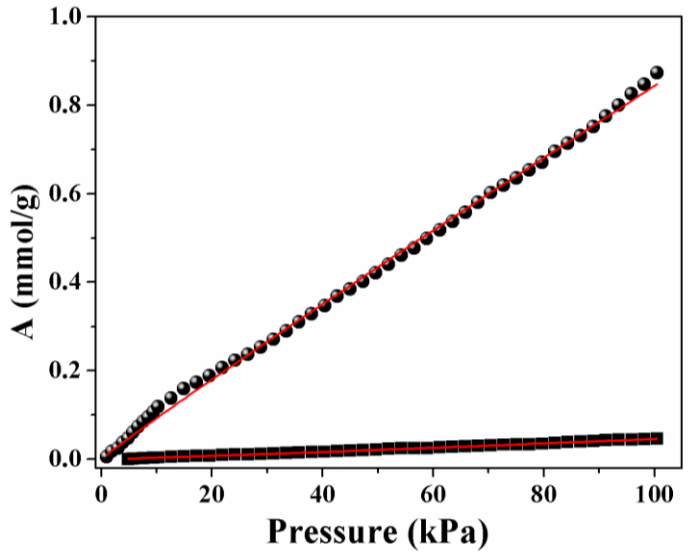

Figure S22: Langmuir-Freundlich fittings (red lines) for (a) C_2H_2 (black circle) and (b) C_2H_6 (black Square) isotherms measured at 293 K for **2IRa**.

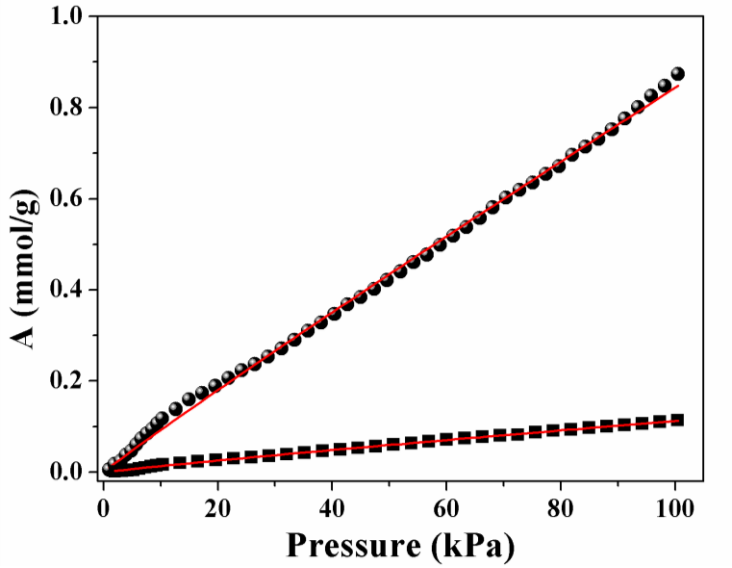

Figure S23: Langmuir-Freundlich fittings (red lines) for (a) C_2H_2 (black circle) and (b) CH_4 (black Square) isotherms measured at 293 K for **2IRa**.

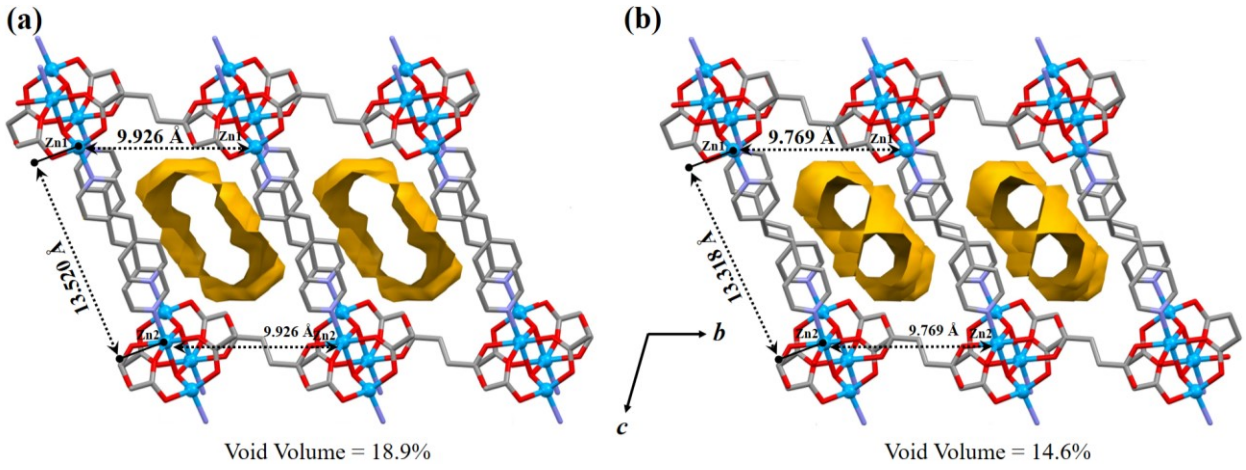

Figure S24: Connolly surface of **2** (a) and **2IR** (b) drawn in the Mercury software with a probe radius of 1.2 Å. After the [2+2] cycloaddition reaction, pore shrinkage has been observed in the photoirradiated framework which is also reflected by the decrease in the void volume.

Column Breakthrough Experiment:

The performance of **2a** in the actual adsorption-based separation and purification process of acetylene from C_2H_2/C_2H_4 mixtures containing 1% acetylene was examined through

experimental column breakthrough (See Fig. S10 of ref S7)[8] in which a C_2H_2/C_2H_4 (1:99, v/v) mixture was flowed through a packed column of **2a** with a total flow rate of 2.2 mL min^{-1} at 293 K. C_2H_4 molecules were detected at the output of the column after 2.3 min of starting the gas flow through **2a** whereas no trace of C_2H_2 was found upto 7.2 min. After that, C_2H_2 molecules slowly started releasing from the outlet which was saturated after 17 min. The efficient purification of C_2H_4 from the gas mixture has been successfully achieved with a total C_2H_2 retention time of 7.2 min.

References

1. Blatov, V. A.; Shevchenko, A. P.; Proserpio, D. M., Applied Topological Analysis of Crystal Structures with the Program Package ToposPro. *Cryst. Growth Des.*, **2014**, *14*, 3576-3586.
2. Dincă, M.; Dailly, A.; Liu, Y.; Brown, C. M.; Neumann, D. A.; Long, J. R., Hydrogen Storage in a Microporous Metal−Organic Framework with Exposed Mn^{2+} Coordination Sites. *J. Am. Chem. Soc.*, **2006**, *128*, 16876-16883.
3. Bae, Y.-S.; Mulfort, K. L.; Frost, H.; Ryan, P.; Punnathanam, S.; Broadbelt, L. J.; Hupp, J. T.; Snurr, R. Q., Separation of CO_2 from CH_4 Using Mixed-Ligand Metal−Organic Frameworks. *Langmuir*, **2008**, *24*, 8592-8598.
4. Myers, A. L.; Prausnitz, J. M., Thermodynamics of mixed-gas adsorption. *AlChE J.*, **1965**, *11*, 121-127.
5. Huang, Y.-L.; Gong, Y.-N.; Jiang, L.; Lu, T.-B., A unique magnesium-based 3D MOF with nanoscale cages and temperature dependent selective gas sorption properties. *Chem. Commun.*, **2013**, *49*, 1753-1755.
6. Liu, B.; Smit, B., Comparative Molecular Simulation Study of CO_2/N_2 and CH_4/N_2 Separation in Zeolites and Metal−Organic Frameworks. *Langmuir*, **2009**, *25*, 5918-5926.
7. Babarao, R.; Hu, Z.; Jiang, J.; Chempath, S.; Sandler, S. I., Storage and Separation of CO_2 and CH_4 in Silicalite, C168 Schwarzite, and IRMOF-1: A Comparative Study from Monte Carlo Simulation. *Langmuir*, **2007**, *23*, 659-666.
8. Hazra, A.; Jana, S.; Bonakala, S.; Balasubramanian, S.; Maji, T. K., Separation/purification of ethylene from an acetylene/ethylene mixture in a pillared-layer porous metal–organic framework. *Chem. Commun.*, **2017**, *53*, 4907-4910.